



A study for multi-layer skin burn injuries based on DPL bioheat model

Rajneesh Kumar Chaudhary¹ · Kabindra Nath Rai² · Jitendra Singh¹

Received: 19 August 2019 / Accepted: 15 June 2020 / Published online: 5 August 2020
© Akadémiai Kiadó, Budapest, Hungary 2020, corrected publication 2020

Abstract

In this paper, multi-layer skin burn injuries are studied using the DPL bioheat model when skin surface is subjected to different non-Fourier boundary conditions. A skin made of three layers known as epidermis, dermis, and subcutaneous layer. These layers assumed to be homogeneous and each layer studied separately. The metabolic heat varies linearly with temperature. The diffusion and evaporation of water in the multi-layer of skin increases heat loss in the skin layer. To solve the BVP of hyperbolic PDE, the FELWG method has been used. The whole analysis presented in a non-dimensional form and the results are shown graphically. In a particular case, the result obtained is compared with the exact solution and is in good agreement. The effects of relaxation time, layer thickness, different temperature, and non-Fourier boundary condition are analyzed at the temperature of the tissue related to the burning of the skin, and the three layers are discussed in detail.

Keywords Dual-phase lagging (DPL) · Finite element Legendre wavelet Galerkin method (FELWGM) · Generalized non-Fourier boundary condition · Multi-layer skin burn

List of symbols

c_p	Specific heat/J kg ⁻¹ °C ⁻¹
k	Thermal conductivity/W m ⁻¹ °C ⁻¹
t	Time/s
T	Temperature/°C
D_f	Coefficient of water diffusion in tissue/m ² s ⁻¹
M_w	The molar mass of water/18 g mol ⁻¹
RH	Relative humidity/%
P_w	Vapor pressure of water/Pa
r	Space coordinate/m
ΔH_{vap}	Enthalpy of water vaporization/2408 J kg ⁻¹
Δm	Water vaporization rate from the skin surface/g m ⁻² s ⁻¹
Δr	Body core distance from current tissue position/m
δc	The average distance of the momentum boundary layer/m
ρ	Density of skin/kg m ⁻³

R_a	Universal gas constant/8.314 J mol ⁻¹ °C ⁻¹
τ_q	Phase lag of heat flux/s
τ_t	Phase lag due to temperature gradient/s
T_w	Wall temperature at the boundary/°C
H	Coefficient of reference heat transfer/W m ⁻² °C ⁻¹
q_w	Reference heat flux/W m ⁻²
T_s	Ambient temperature/°C
Q_v	Evaporation of water
Q_d	Diffusion of water

Subscripts and superscripts

b	Blood
c	Core
a	Air
f	Diffusion of water
m	Metabolic production
s	Surface of skin
v	Vaporization
W	Water

Non-dimensional variable

F_o	Non-dimensional time
x	Non-dimensional space coordinate
K_i	Kirchhoff number
B_i	Biot number
F_{ot}	Non-dimensional phase lag due to temperature gradient
F_{oq}	Non-dimensional phase lag of heat flux

✉ Jitendra Singh
jitendraprof@gmail.com

Rajneesh Kumar Chaudhary
kingrajneesh222kumar@gmail.com

Kabindra Nath Rai
knrai.apm@itbhu.ac.in

¹ Department of Mathematics, Institute of Science, Banaras Hindu University, Varanasi 221005, India

² Department of Mathematical Sciences, IIT-BHU, Varanasi 221005, India

P_{mo}	Non-dimensional coefficient of metabolic heat source
P_f	Non-dimensional coefficient of blood perfusion
θ	Non-dimensional tissue temperature
θ_s	Non-dimensional fluid temperature
θ_w	Non-dimensional wall temperature of the tissue
θ_b	Non-dimensional blood temperature

Introduction

Thermal damage to the skin is the most common damage to civilians and military people. In medical treatment, by heat transmitted to damage the cancerous tissue without affecting the normal tissue, hyperthermia treatment under a control temperature distribution should have a cancer cell distorted. For medical treatment, it is necessary to detect heat distribution in biological tissue. There is also thermal damage to the skin in a hot (like Desert) and cold (like Mountain) climate. Many researchers use different forms of bioheat models (Pennes [1], Weinbaum and Jiji [2], Nakayama and Kuwahara [3]) to study the thermal behavior in skin tissue. In Pennes model, the temperature gradient in organic tissue is obtained by classical Fourier's law which is

$$q(r, t) = -k\nabla T(r, t), \quad (1)$$

where heat flux $q(r, t)$ and the temperature gradient $\nabla T(r, t)$ are at the arbitrary point of tissue.

The Pennes bioheat model [1] is a commonly used model to simulate the study of the thermal behavior of body tissues, which includes metabolic heat and blood perfusion. Shen et al [4] considered the heat and mass transfers in skin models with the diffusion of water and vaporization, but Ming stated that it is different for each layer, which is not considered in the Shen model. Analysis of the numerical skin model was defined for multi-layer (i.e., solder, epidermis, dermis, and fatty tissue), using laser coupled on human skin [5]. The layer of each skin is assigned to the properties of initial optical, thermal, and water density, and the water content in each layer is calculated from diffusion, where water loss occurs by evaporation. The blood perfusion, the diffusion of water, and the heat of metabolism remain in all three layers except the perfusion of blood are not present in the epidermis layer. The dynamic temperature and distribution for the multi-layer have been defined. Physical parameters affect burning injuries, i.e., thickness of epidermis and dermis tissue, the thermal conductivity of the dermis and subcutaneous tissue. The capacity of heat, blood perfusion rate, and the diffusion of water have very little effect on epidermis and dermis layer. To analyze skin burn at high temperatures, Ming [6, 7] introduces a one dimension

multi-layer skin model and obtained temperature distribution using a finite volume method which is found to be good with experimental. The results show very little effect of temperature distribution with variation of blood perfusion and initial temperature on multi-layer skin models. Metabolic heat in the skin model was considered to be zero by Ming et. al. [6, 7], but it is experimental that it has a significant effect on skin.

A mathematical model is considered for measuring the blood perfusion rate in local tissue by using Pennes equation [8]. Two parameters are difficult to know, i.e., T_a is arterial blood temperature and Q_m is the metabolic heat generation rate has been eliminated for evaluating W_b is the local perfusion rate in the tissue. In the novel, a noninvasive method for laser Lipolysis and the heating and cooling behavior occurring in laser Lipolysis was studied [9]. In the theoretical model, laser Lipolysis that helped by cooling the skin was investigated by establishing a homogeneous multi-layer skin model that included the epidermis, dermis, and subcutaneous layer.

In biological tissue, a classical Fourier law describes a mathematical model for the study of heat transfer. In this model, during the thermal therapy of electromagnetic radiation, a separate coordination system and various boundary conditions are studied [10]. Galerkin's method is used to solve the problem with Bernstein polynomial as a basis function [11]. They discussed the effect of the parameters P_f , P_m , P_r , K_i and B_i on the tissue and found that the condition of the boundary and internal heat in the human body during thermal therapy is not equal, that is, changes in organ from one organ to another.

The classical Fourier law is not good for heat transfer in biological tissue. Heat always promotes with biological tissue at the time of relaxation with finite speed. A thermal wave model approach has been introduced based on relaxation time known as the non-classical Fourier bioheat model. After removing, the paradox Cattaneo [12] and Vernotte [13] introduced SPL bioheat model as follows:

$$q(r, t + \tau_q) = -k\nabla T(r, t). \quad (2)$$

This theoretically examines the thermal behavior in the living tissue of the thermal wave model, which is under continuous, sinusoidal, or phase surface heating. The heat mainly spreads in the direction of the skin vertically. The effects of thermal physical properties were discussed on wave model heat transfer. The problem has been solved using a modified discretization scheme based on the Laplace transform [14].

A mathematical model is considered for non-Fourier (SPL) heat transfer in tumor or cancer tissue [15] and a non-Fourier (SPL) heat mass transfer within the food items under generalized boundary conditions [16]. In these

mathematical models, a finite difference technique is used for discretization in space, and the non-dimensional boundary value problem has been solved by the Legendre Wavelet basis function and compared to the results obtained by the Legendre Galerkin Wavelet method, with exact solutions and found in good agreement ($\tau_q = 0$). They discussed the variability of time, the location of tumors or cancer, relaxation time, temperature distribution, etc.

This mathematical model [17] is based on the implementation of Cattaneo Christov heat flux for single and multi-walled-type carbon nanotubes with considering water as based fluid. The effect of thermal Biot numbers on fluid temperature is discussed and found a higher value of thermal relaxation parameter results in gradual retardation in the temperature profile.

The delay between the heat flux and temperature gradient is known as thermal relaxation time. However, due to micro-scale responses from time to time, the thermal wave model of bioheat transfer has not captured the microscale reactions in space. Due to this, it produces some unusual behavior of thermal diffusion. To consider the effect of rapid transient effects along with the effect of microstructural interaction, a phase interval for the temperature gradient has introduced another relaxation time τ_t [18, 19],

$$q(r, t + \tau_q) = -k\nabla T(r, t + \tau_t), \quad (3)$$

and the respective model is called the dual-phase lagging (DPL) model. A DPL model is applied to the principle of porous media and non-balance heat transfer in organic tissues by Zhang [20]. In this work, phase lag times have been expressed as coupling factors, porosity, thermal conductivity of tissues and blood, and capacity of heat. If $\tau_t = 0$, then DPL model changed in SPL model and if $\tau_q = 0$, $\tau_t = 0$, then DPL model changed in classical Fourier model.

A mathematical model is considered as a DPL model of bioheat transfer, under generalized boundary condition, and hyperthermia treatment is studied by using the term Gaussian distribution source [21]. During the treatment of hyperthermia, the Gaussian distribution source helps in controlling the temperature, which makes this study more useful in the field of clinical therapeutic for prediction and control of temperature.

During theoretical thermal therapy, thermal behavior is examined under various non-Fourier boundary condition in living biological tissue with the DPL bioheat transfer model. The properties of the Legendre wavelet are utilized to obtain an estimated analytical solution to the problem, together with a finite difference scheme. It has been observed that when it is used with a spherical symmetrical coordination

system, the second and third kinds of boundary condition are less affected to the surrounding tissues [22].

The time-fractional nonlinear dispersive partial differential equations in the sense of conformable fractional derivative are proposed. The solitary pattern solution to the problem is based on the residual fractional power series and homotopy asymptotic method. The results show that the algorithm is based on Taylor series approximations of the nonlinear equations in a rapid convergence series leading to ideal solutions [23, 24].

A comparative study of the Newell–Whitehead–Segel and nonlinear Kaup–Kupershmidt equations, this equation is solved by a modified analytical technique based on auxiliary parameters, residual power series method, and numerical approximations with the integral recursive scheme [25, 26]. A coupled nonlinear partial differential equations for momentum and conservation of energy are transformed into coupled nonlinear ordinary differential equations using exact similarity transformations, which are known as Cattaneo–Christov heat flux model for third-grade viscoelastic power-law non-Newtonian fluid [27]. A systematic analysis of boundary-layer flow depends on various parameters including Prandtl number, power index, and temperature variation coefficient and shows the effect of these parameters on the velocity and temperature profiles.

Theoretical analysis and a comprehensive experimental investigation of thermal and fire properties were performed in the work using thermogravimetric analysis, cone calorimeters, limiting oxygen index, vertical/horizontal burning tests, and scanning electron microscope tests [28]. Kleilton et al. [29] analysis concluded that the films fit the biological system. Thermal, physical, chemical, and mechanical stability are the same, and instability of the material is caused by the addition of charges in the chitosan polymer matrix.

Henze et al. [30] have analyzed the effect of thermal barrier coating for separation from hot gas. They explained the general behavior of the effect of the thermal barrier coating Biot number on the effective heat transfer coefficient. Biot number increases with increase in the Reynolds number, and the ratio between the pure hot gas and the effective heat transfer coefficient is increased. The conduction and convection heat transfer mechanisms were studied by [31] and also considering the importance of heat transfer parameters, i.e., Rayleigh number, Stefan number, Biot number, etc.

In the present study, we discussed the thermal behavior of the DPL model to skin tissues under the most generalized non-Fourier boundary condition. Using the discretization in space coordination, the problem with the initial condition is changed into the system of O.D.E's. The unknown variables in the system of O.D.E's are resolved using FELWGM, which

converts the system into a Sylvester equation. Solving this Sylvester's equation by using MATLAB software, the solution obtained is used for non-dimensional temperature distribution and various effects on the skin layer are analyzed.

Description of physical problem

A multi-layer model on the skin is established including lagging behavior and the thermal behaviors of the skin during simulating. The skin made of three layers, i.e., epidermis, dermis, and subcutaneous tissue, is shown in Fig. 1. Every layer assumes to be homogeneous and considers the heat transfer in the skin with metabolic heat Q_m , water diffusion Q_d , and vaporization Q_v . Metabolic heat is generated in the skin tissues due to various physical processes occurring in the body [15]. Blood perfusion is a convection term produced by the flow of blood [15]. All three-layer contain metabolic heat and diffusion of water. Blood perfusion occurs in three layers except the epidermis layer. Water present inside the skin tissue could be vaporized due to temperature, but vaporization occurs only outer surface, i.e., epidermis layer [5].

Formulation of problem

The Fourier heat transfer model of multi-layer of tissue is given below [6, 7]:

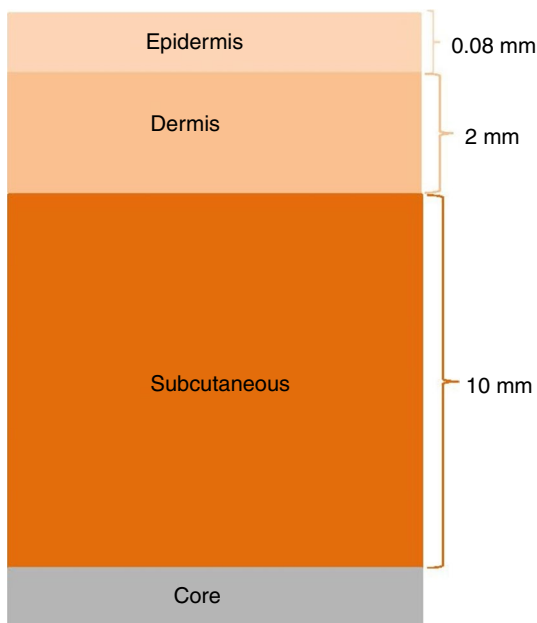


Fig. 1 Multi-layer of human skin

Epidermis layer:

$$\rho c_p \frac{\partial T(r, t)}{\partial t} = k \nabla^2 T(r, t) + Q_m - Q_v - Q_d, \tag{4}$$

Dermis layer:

$$\begin{aligned} \rho c_p \frac{\partial T(r, t)}{\partial t} &= k \nabla^2 T(r, t) + Q_m - Q_d \\ &+ \rho_b c_{pb} w_b (T_b - T(r, t)), \end{aligned} \tag{5}$$

Subcutaneous layer:

$$\begin{aligned} \rho c_p \frac{\partial T(r, t)}{\partial t} &= k \nabla^2 T(r, t) + Q_m - Q_d \\ &+ \rho_b c_{pb} w_b (T_b - T(r, t)). \end{aligned} \tag{6}$$

After applying lagging in both space and time in the Fourier model of multi-layer, i.e., also called a DPL model of multi-layer, which is given below:

Epidermis layer:

$$\begin{aligned} \tau_q \rho c_p \frac{\partial^2 T(r, t)}{\partial t^2} - \tau_q \frac{\partial Q_m}{\partial t} + \tau_q \frac{\partial Q_d}{\partial t} + \rho c_p \frac{\partial T(r, t)}{\partial t} \\ = k \nabla^2 \left[T(r, t) + \tau_t \frac{\partial T(r, t)}{\partial t} \right] + Q_m - Q_v - Q_d, \end{aligned} \tag{7}$$

Dermis layer:

$$\begin{aligned} \tau_q \rho c_p \frac{\partial^2 T(r, t)}{\partial t^2} - \tau_q \frac{\partial Q_m}{\partial t} + \tau_q \frac{\partial Q_d}{\partial t} + \rho c_p \frac{\partial T(r, t)}{\partial t} \\ + \tau_q \rho_b c_{pb} w_b \frac{\partial T(r, t)}{\partial t} = k \nabla^2 \left[T(r, t) + \tau_t \frac{\partial T(r, t)}{\partial t} \right] \\ + Q_m - Q_d + \rho_b c_{pb} w_b (T_b - T(r, t)), \end{aligned} \tag{8}$$

Subcutaneous layer:

$$\begin{aligned} \tau_q \rho c_p \frac{\partial^2 T(r, t)}{\partial t^2} - \tau_q \frac{\partial Q_m}{\partial t} + \tau_q \frac{\partial Q_d}{\partial t} + \rho c_p \frac{\partial T(r, t)}{\partial t} \\ + \tau_q \rho_b c_{pb} w_b \frac{\partial T(r, t)}{\partial t} = k \nabla^2 \left[T(r, t) + \tau_t \frac{\partial T(r, t)}{\partial t} \right] \\ + Q_m - Q_d + \rho_b c_{pb} w_b (T_b - T(r, t)), \end{aligned} \tag{9}$$

$$Q_m = Q_{mo} \left\{ 1 + \frac{(T(r,t) - T_0)}{10} \right\}, \tag{10}$$

$$Q_d = \frac{D_f c_{pW} (\rho_s - \rho_c)}{(\Delta r)^2} (T(r, t) - T_0), \tag{11}$$

$$Q_v = \frac{\Delta m \Delta H_{vap}}{\delta c}, \tag{12}$$

$$\Delta m = \frac{D_v M_W}{R_a \delta c} \left[\left(\frac{P_W}{T_W} \right)_s - \left(\frac{P_W}{T_W} \right)_a RH \right], \tag{13}$$

where the term Q_{mo} is constant metabolic heat, blood perfusion rate w_b , blood density ρ_b is taken as 1060 kg m^{-3} , blood specific heat c_{pb} is taken as $3770 \text{ J kg}^{-1} \text{ }^\circ\text{C}^{-1}$ [33] and blood temperature T_b is taken as equal to core temperature T_0 (37°C). The average water vapor diffusivity and specific heat of water are D_v and c_{pW} respectively. The water content in the core body and skin layer are ρ_c and ρ_s , respectively. The thermal physical properties of three skin layer are shown in Table 1 [6, 7].

The associated initial conditions for DPL skin model are

$$T(r, 0) = T_0, \tag{14}$$

$$\frac{\partial T(r, 0)}{\partial t} = 0, \tag{15}$$

generalized non-Fourier boundary condition

$$A' \frac{\partial}{\partial r} \left[T(0, t) + \tau_t \frac{\partial T(0, t)}{\partial t} \right] + B' T(0, t) = f(t), \tag{16}$$

for the first kind non-Fourier boundary condition: $A' = 0, B' = 1, f(t) = T_w$,

for the second kind non-Fourier boundary condition: $A' = -k, B' = 0, f(t) = q_w$, for the third kind non-Fourier boundary condition: $A' = -k, B' = H, f(t) = H T_s$, and non-Fourier symmetric condition

$$\frac{\partial}{\partial r} \left[T(R, t) + \tau_t \frac{\partial T(R, t)}{\partial t} \right] = 0. \tag{17}$$

Skin burn of model

The temperature of the epidermis or dermis or subcutaneous will cause damage to the skin reaches 44°C [36]. According to the first-order process of a chemical reaction,

$$\frac{d\Omega}{dt} = \begin{cases} 0 & T(r, t) < 44^\circ\text{C, i.e. no burn,} \\ P e^{\frac{\Delta E}{RT}} & T(r, t) \geq 44^\circ\text{C, i.e. burn.} \end{cases}$$

First, second, and third-degree burn occurred, if damage function Ω reaches values of 0.53, 1.0 and 10^4 , respectively [37]. P and ΔE [38] values are selected according to the prediction of skin burning [6, 7].

Non-dimensional quantities

Introducing the non-dimensional parameter and similarity criteria $\theta(x, F_o) = \frac{T(r,t) - T_0}{T_0}, F_o = \frac{kt}{\rho c_p R^2}, x = \frac{r}{R}, \theta_b = \frac{T_b - T_0}{T_0}, \theta_w = \frac{T_w - T_0}{T_0}, \theta_s = \frac{T_s - T_0}{T_0}, F_{oq} = \frac{k \tau_q}{\rho c_p R^2}, F_{ot} = \frac{k \tau_t}{\rho c_p R^2}, P_f = \sqrt{\frac{w_b c_{pb} \rho_b}{k}} R, P_{mo} = \frac{Q_{mo} R^2}{k T_0}, \alpha = 0.1 \times T_0 Q_{vo} = \frac{\Delta m \cdot \Delta H_{vap}}{\delta c} \frac{R^2}{k T_0}, Q_{do} = \frac{D_f c_{pW} (\rho_s - \rho_c)}{(\Delta r)^2} \frac{R^2}{k}, f(F_o) = \frac{f(t) - B' T_0}{T_0}, A = \frac{A'}{R}, B = B', K_i = \frac{q_w R}{T_0 k}, B_i = \frac{HR}{k}$. Equations (7–17) are converted into non-dimensional form as follows: Epidermis layer:

$$F_{oq} \frac{\partial^2 \theta(x, F_o)}{\partial F_o^2} + (1 - F_{oq} \alpha P_{mo} + F_{oq} Q_{do}) \frac{\partial \theta(x, F_o)}{\partial F_o} = \frac{\partial^2}{\partial x^2} \left[\theta(x, F_o) + F_{ot} \frac{\partial \theta(x, F_o)}{\partial F_o} \right] + (\alpha P_{mo} - Q_{do}) \theta(x, F_o) + P_{mo} - Q_{vo}, \tag{18}$$

Dermis layer:

Table 1 Physical and thermal properties of the skin layer [6, 7]

Physical parameters	Epidermis	Dermis	Subcutaneous	References
Diffusivity of water/mm ² s ⁻¹	5×10^{-4}	5×10^{-4}	5×10^{-4}	[5, 32]
Density/kg m ⁻³	1200	1200	1000	[33]
Thermal conductivity/W m ⁻¹ °C ⁻¹	0.24	0.45	0.19	[34, 35]
Thickness/mm	0.08	2.0	10	[34, 35]
Rate of blood perfusion/s ⁻¹	0	0.00125	0.00125	[34, 35]
Specific heat/J kg ⁻¹ k ⁻¹	3590	3330	2500	[34, 35]
Water content/%	70	70	20	[5]

$$F_{oq} \frac{\partial^2 \theta(x, F_o)}{\partial F_o^2} + (1 - F_{oq} \alpha P_{mo} + F_{oq} Q_{do} + F_{oq} P_f^2) \frac{\partial \theta(x, F_o)}{\partial F_o} = \frac{\partial^2}{\partial x^2} \left[\theta(x, F_o) + F_{ot} \frac{\partial \theta(x, F_o)}{\partial F_o} \right] + (\alpha P_{mo} - Q_{do} - P_f^2) \theta(x, F_o) + (P_{mo} + P_f^2 \theta_b), \tag{19}$$

Subcutaneous layer:

$$F_{oq} \frac{\partial^2 \theta(x, F_o)}{\partial F_o^2} + (1 - F_{oq} \alpha P_{mo} + F_{oq} Q_{do} + F_{oq} P_f^2) \frac{\partial \theta(x, F_o)}{\partial F_o} = \frac{\partial^2}{\partial x^2} \left[\theta(x, F_o) + F_{ot} \frac{\partial \theta(x, F_o)}{\partial F_o} \right] + (\alpha P_{mo} - Q_{do} - P_f^2) \theta(x, F_o) + (P_{mo} + P_f^2 \theta_b). \tag{20}$$

Initial conditions

$$\theta(x, 0) = 0, \tag{21}$$

$$\frac{\partial \theta(x, 0)}{\partial F_o} = 0, \tag{22}$$

generalized non-Fourier boundary condition

$$A \frac{\partial}{\partial x} \left[\theta(0, F_o) + F_{ot} \frac{\partial \theta(0, F_o)}{\partial F_o} \right] + B \theta(0, F_o) = f(F_o), \tag{23}$$

for the first kind non-Fourier boundary condition: $A = 0, B = 1, f(F_o) = \theta_w,$

$$\theta(0, F_o) = F(F_o) = \theta_w, \tag{24}$$

for the second kind non-Fourier boundary condition: $A = 1, B = 0, f(F_o) = -K_i,$

$$\frac{\partial \theta(0, F_o)}{\partial x} = F(F_o) = -K_i(1 - e^{-\frac{F_o}{F_{ot}}}), \tag{25}$$

(see Appendix ‘‘Second kind non-Fourier boundary condition’’),

for the third kind non-Fourier boundary condition: $A = 1, B = -B_i, f(F_o) = -B_i \theta_s,$

$$\frac{\partial \theta(0, F_o)}{\partial x} = F(F_o) = -B_i(\theta_s - \theta(0, F_o))(1 - e^{-\frac{F_o}{F_{ot}}}), \tag{26}$$

(see Appendix ‘‘Third kind non-Fourier boundary condition’’),

and non-Fourier symmetric condition

$$\frac{\partial}{\partial x} \left[\theta(1, F_o) + F_{ot} \frac{\partial \theta(1, F_o)}{\partial F_o} \right] = 0, \tag{27}$$

(see Appendix ‘‘Non-Fourier symmetric condition’’).

Numerical solution of the problem

By finite difference scheme, we discretized the domain in space variable x . Let the grid size, $x = h = 1/k \geq 0$ and grid points are taken in the space interval $[0, 1]$ are the numbers $x_j = jh, j = 1, 2, \dots, k$. The non-dimensional temperature θ at points x_j is indicated by $\theta_j(F_o) = \theta(x_j, F_o)$, for $F_o \geq 0$. We used central difference scheme for second order derivative.

After simple algebraic computation, Eqs. (18–27) change the system into vector matrix as follows:

Epidermis layer:

$$F_{oq} \frac{d^2 \theta_j(F_o)}{dF_o^2} + (1 - F_{oq} \alpha P_{mo} + F_{oq} Q_{do}) \frac{d\theta_j(F_o)}{dF_o} = \frac{1}{h^2} [\theta_{j+1}(F_o) - 2\theta_j(F_o) + \theta_{j-1}(F_o)] + F_{ot} \frac{d}{dF_o} \left[\frac{1}{h^2} \{ \theta_{j+1}(F_o) - 2\theta_j(F_o) + \theta_{j-1}(F_o) \} \right] + (\alpha P_{mo} - Q_{do}) \theta_j(F_o) + N_{1j}, \tag{28}$$

Dermis layer:

$$F_{oq} \frac{d^2 \theta_j(F_o)}{dF_o^2} + (1 - F_{oq} \alpha P_{mo} + F_{oq} Q_{do} + F_{oq} P_f^2) \frac{d\theta_j(F_o)}{dF_o} = \frac{1}{h^2} [\theta_{j+1}(F_o) - 2\theta_j(F_o) + \theta_{j-1}(F_o)] + F_{ot} \frac{d}{dF_o} \left[\frac{1}{h^2} (\theta_{j+1}(F_o) - 2\theta_j(F_o) + \theta_{j-1}(F_o)) \right] + (\alpha P_{mo} - Q_{do} - P_f^2) \theta_j(F_o) + N_{2j}, \tag{29}$$

Subcutaneous layer:

$$F_{oq} \frac{d^2 \theta_j(F_o)}{dF_o^2} + (1 - F_{oq} \alpha P_{mo} + F_{oq} Q_{do} + F_{oq} P_f^2) \frac{d\theta_j(F_o)}{dF_o} = \frac{1}{h^2} [\theta_{j+1}(F_o) - 2\theta_j(F_o) + \theta_{j-1}(F_o)] + F_{ot} \frac{d}{dF_o} \left[\frac{1}{h^2} (\theta_{j+1}(F_o) - 2\theta_j(F_o) + \theta_{j-1}(F_o)) \right] + (\alpha P_{mo} - Q_{do} - P_f^2) \theta_j(F_o) + N_{3j}, \tag{30}$$

with initial conditions

$$\theta_j(0) = 0, \frac{d\theta_j(0)}{dF_o} = 0. \tag{31}$$

Using four-point formula [39], boundary points given as

$$\frac{\partial \theta}{\partial x} \Big|_{x=0} = \frac{1}{20h} [-21 \theta_0 + 13 \theta_1 + 17 \theta_2 - 9 \theta_3], \tag{32}$$

$$\frac{\partial \theta}{\partial x} \Big|_{x=1} = \frac{1}{20h} [21 \theta_{k+1} - 13 \theta_k - 17 \theta_{k-1} + 9 \theta_{k-2}]. \tag{33}$$

Using vector-matrix notation, Eqs. (28–30) can be written in the more compact form

Epidermis layer:

and

$$\frac{d\theta(0)}{dF_o} = \left[\frac{d\theta_1(0)}{dF_o} \quad \frac{d\theta_2(0)}{dF_o} \quad \dots \quad \frac{d\theta_k(0)}{dF_o} \right]^T = [0 \ 0 \ \dots \ 0]^T, \tag{39}$$

order of matrix M is $k \times k$ and order of matrix $\theta, N_1, N_2,$ and N_3 are $k \times 1$, where

$$M = M_l \begin{cases} l = 1 & \text{for first kind non-Fourier boundary condition,} \\ l = 2 & \text{for second kind non-Fourier boundary condition,} \\ l = 3 & \text{for third kind non-Fourier boundary condition.} \end{cases} \tag{40}$$

$$F_l(F_o) = \begin{cases} \theta_w & l = 1, \text{ for first kind non-Fourier boundary condition,} \\ \frac{20h K_1(1-e^{-\frac{F_o}{F_{ot}}})}{21} & l = 2, \text{ for second kind non-Fourier boundary condition,} \\ \frac{20h B_1(\theta_s - \theta(0, F_o))(1-e^{-\frac{F_o}{F_{ot}}})}{21} & l = 3, \text{ for third kind non-Fourier boundary condition.} \end{cases} \tag{41}$$

$$\begin{aligned} F_{oq} \frac{d^2 \theta(F_o)}{dF_o^2} + (1 - F_{oq} \alpha P_{mo} + F_{oq} Q_{do}) \frac{d\theta(F_o)}{dF_o} \\ = M \theta(F_o) + F_{ot} \frac{d(M \theta(F_o))}{dF_o} \\ + (\alpha P_{mo} - Q_{do}) \theta(F_o) + N_1, \end{aligned} \tag{34}$$

Dermis layer:

$$\begin{aligned} F_{oq} \frac{d^2 \theta(F_o)}{dF_o^2} + (1 - F_{oq} \alpha P_{mo} + F_{oq} Q_{do} + F_{oq} P_f^2) \frac{d\theta(F_o)}{dF_o} \\ = M \theta(F_o) + F_{ot} \frac{d(M \theta(F_o))}{dF_o} \\ + (\alpha P_{mo} - Q_{do} - P_f^2) \theta(F_o) + N_2, \end{aligned} \tag{35}$$

Subcutaneous layer:

$$\begin{aligned} F_{oq} \frac{d^2 \theta(F_o)}{dF_o^2} \\ + (1 - F_{oq} \alpha P_{mo} + F_{oq} Q_{do} + F_{oq} P_f^2) \frac{d\theta(F_o)}{dF_o} \\ = M \theta(F_o) + F_{ot} \frac{d(M \theta(F_o))}{dF_o} \\ + (\alpha P_{mo} - Q_{do} - P_f^2) \theta(F_o) + N_3, \end{aligned} \tag{36}$$

where

$$\theta = [\theta_1 \theta_2 \dots \theta_k]^T, \tag{37}$$

with initial condition

$$\theta(0) = [\theta_1(0) \theta_2(0) \dots \theta_k(0)]^T = [0 \ 0 \ \dots \ 0]^T, \tag{38}$$

$$M_1 = \frac{1}{h^2} \begin{bmatrix} -2 & 1 & 0 & \dots & 0 & 0 & 0 \\ 1 & -2 & 1 & \dots & 0 & 0 & 0 \\ 0 & 1 & -2 & \dots & 0 & 0 & 0 \\ \cdot & \cdot & \cdot & \dots & \cdot & \cdot & \cdot \\ \cdot & \cdot & \cdot & \dots & \cdot & \cdot & \cdot \\ 0 & 0 & 0 & \dots & 1 & -2 & 1 \\ 0 & 0 & 0 & \dots & \frac{-9}{21} & \frac{38}{21} & \frac{-29}{21} \end{bmatrix}, \tag{42}$$

$$M_2 = \frac{1}{h^2} \begin{bmatrix} \frac{-29}{21} & \frac{38}{21} & \frac{-9}{21} & \dots & 0 & 0 & 0 \\ 1 & -2 & 1 & \dots & 0 & 0 & 0 \\ 0 & 1 & -2 & \dots & 0 & 0 & 0 \\ \cdot & \cdot & \cdot & \dots & \cdot & \cdot & \cdot \\ \cdot & \cdot & \cdot & \dots & \cdot & \cdot & \cdot \\ 0 & 0 & 0 & \dots & 1 & -2 & 1 \\ 0 & 0 & 0 & \dots & \frac{-9}{21} & \frac{38}{21} & \frac{-29}{21} \end{bmatrix}, \tag{43}$$

$$M_3 = \frac{1}{h^2} \begin{bmatrix} \frac{-29}{21} & \frac{38}{21} & \frac{-9}{21} & \dots & 0 & 0 & 0 \\ 1 & -2 & 1 & \dots & 0 & 0 & 0 \\ 0 & 1 & -2 & \dots & 0 & 0 & 0 \\ \cdot & \cdot & \cdot & \dots & \cdot & \cdot & \cdot \\ \cdot & \cdot & \cdot & \dots & \cdot & \cdot & \cdot \\ 0 & 0 & 0 & \dots & 1 & -2 & 1 \\ 0 & 0 & 0 & \dots & \frac{-9}{21} & \frac{38}{21} & \frac{-29}{21} \end{bmatrix}, \tag{44}$$

$$N_1 = \left[P_{mo} - Q_{vo} + \frac{F_l(F_o)}{h^2} P_{mo} - Q_{vo} \dots P_{mo} - Q_{vo} \right]^T, \tag{45}$$

$$N_2 = \left[P_{mo} + P_f^2 \theta_b + \frac{F_i(F_o)}{h^2} P_{mo} + P_f^2 \theta_b \dots P_{mo} + P_f^2 \theta_b \right]^T, \tag{46}$$

$$N_3 = \left[P_{mo} + P_f^2 \theta_b + \frac{F_i(F_o)}{h^2} P_{mo} + P_f^2 \theta_b \dots P_{mo} + P_f^2 \theta_b \right]^T. \tag{47}$$

Finite element Legendre wavelet Galerkin method

To solve the system of ordinary differential Eqs. (34–39), let us consider

$$\frac{d^2 \theta(F_o)}{dF_o^2} = C_y^T \psi(F_o), \tag{48}$$

where $y = 1, 2$, and 3 for epidermis, dermis, and subcutaneous layer, respectively, C_y^T is unknown coefficient matrix of order $2^{k-1}M' \times 2^{k-1}M'$, and $\psi(F_o)$ is a column vector of $2^{k-1}M' \times 1$,

$$\psi(F_o) = \left[\begin{matrix} \psi_{10} & \psi_{11} & \dots & \psi_{1M'-1} & \psi_{20} & \psi_{21} & \dots & \psi_{2M'-1} & \psi_{2k-10} \\ & \psi_{2k-11} & \dots & \psi_{2k-1M'-1} & & & & & \end{matrix} \right]^T \tag{49}$$

Legendre Wavelets $\psi_{nm}(F_o) = \psi(k, \hat{n}, m, F_o)$ by Razzaghi and Yousefi [40] in $[0, 1)$ have four arguments,

$$L = \left[\begin{matrix} 1 & \frac{1}{\sqrt{3}} & 0 & 0 & \dots & 0 & 0 \\ -\frac{1}{\sqrt{3}} & 0 & \frac{1}{\sqrt{15}} & 0 & \dots & 0 & 0 \\ 0 & -\frac{1}{\sqrt{15}} & 0 & \frac{1}{\sqrt{35}} & \dots & 0 & 0 \\ 0 & 0 & -\frac{1}{\sqrt{35}} & 0 & \dots & 0 & 0 \\ \dots & \dots & \dots & \dots & \dots & \dots & \dots \\ \dots & \dots & \dots & \dots & \dots & \dots & \dots \\ 0 & 0 & 0 & 0 & \dots & 0 & \frac{1}{\sqrt{(2M'-3)(2M'-1)}} \\ 0 & 0 & 0 & 0 & \dots & -\frac{1}{\sqrt{(2M'-1)(2M'-3)}} & 0 \end{matrix} \right]. \tag{55}$$

$k = 2, 3, \dots, \hat{n} = 2n - 1; n = 1, 2, \dots, 2^{k-1}; m = 0, 1, \dots, M' - 1;$ F_o is the normalized time. The Legendre polynomial of order m with mass function $w(F_o) = 1; F_o \in [0, 1]$ formed orthogonal set.

$$\psi_{nm}(F_o) = \begin{cases} \sqrt{(m + \frac{1}{2})2^{\frac{k}{2}}} P_m(2^k F_o - \hat{n}), & \frac{\hat{n}-1}{2^k} \leq F_o \leq \frac{\hat{n}+1}{2^k}, \\ 0 & \text{otherwise,} \end{cases} \tag{50}$$

where $P_0(F_o) = 1, P_1(F_o) = F_o, P_{m+1}(F_o) = \frac{2m+1}{m+1} F_o P_m(F_o) - \frac{m}{m+1} P_{m-1}(F_o)$. Integrating Eq. (48) with respect to F_o , we get

$$\frac{d\theta(F_o)}{dF_o} = C_y^T P \psi(F_o), \tag{51}$$

where P is an operational matrix of order $2^{k-1}M' \times 2^{k-1}M'$. The operational matrix of integration [40] is defined as

$$\int_0^{F_o} \psi(s) ds = P \psi(F_o), F_o \in [0, 1], \tag{52}$$

$$P = \frac{1}{2^k} \begin{bmatrix} L & O & O & \dots & O & O & O \\ 0 & L & O & \dots & O & O & O \\ 0 & 0 & L & \dots & O & O & O \\ \cdot & \cdot & \cdot & \dots & \cdot & \cdot & \cdot \\ \cdot & \cdot & \cdot & \dots & \cdot & \cdot & \cdot \\ 0 & 0 & 0 & \dots & 0 & L & O \\ 0 & 0 & 0 & \dots & 0 & 0 & L \end{bmatrix}, \tag{53}$$

where O and L are the matrix of order $M' - 1 \times M' - 1$ defined as

$$O = \begin{bmatrix} 2 & 0 & 0 & \dots & 0 & 0 & 0 \\ 0 & 0 & 0 & \dots & 0 & 0 & 0 \\ 0 & 0 & 0 & \dots & 0 & 0 & 0 \\ \cdot & \cdot & \cdot & \dots & \cdot & \cdot & \cdot \\ \cdot & \cdot & \cdot & \dots & \cdot & \cdot & \cdot \\ 0 & 0 & 0 & \dots & 0 & 0 & 0 \\ 0 & 0 & 0 & \dots & 0 & 0 & 0 \end{bmatrix}, \tag{54}$$

and

Again integration Eq. (51) with respect to F_o , we get

$$\theta(F_o) = C_y^T P^2 \psi(F_o). \tag{56}$$

Replace the value of $\theta(F_o), \frac{d\theta(F_o)}{dF_o}$ and $\frac{d^2\theta(F_o)}{dF_o^2}$ in Eqs. (34–36) respectively, we get

Epidermis layer:

$$C_1^T - M_l C_1^T X_1 - Z_1 = 0, \tag{57}$$

Dermis layer:

$$C_2^T - M_1 C_2^T X_2 - Z_2 = 0, \tag{58}$$

Subcutaneous layer:

$$C_3^T - M_1 C_3^T X_3 - Z_3 = 0, \tag{59}$$

where $X_1 = (P^2 + F_{ot}P)[(F_{oq}I + (1 - F_{oq}\alpha P_{mo} + F_{oq}Q_{do})P - (\alpha P_{mo} - Q_{do})P^2)]^{-1}$, $Z_1 = N_1 d^T [(F_{oq}I + (1 - F_{oq}\alpha P_{mo} + F_{oq}Q_{do})P - (\alpha P_{mo} - Q_{do})P^2)]^{-1}$, $X_2 = (P^2 + F_{ot}P)[(F_{oq}I + (1 - F_{oq}\alpha P_{mo} + F_{oq}Q_{do} + F_{oq}P_f^2)P - (\alpha P_{mo} - Q_{do} - P_f^2)P^2)]^{-1}$, $Z_2 = N_2 d^T [(F_{oq}I + (1 - F_{oq}\alpha P_{mo} + F_{oq}Q_{do} + F_{oq}P_f^2)P - (\alpha P_{mo} - Q_{do} - P_f^2)P^2)]^{-1}$, $X_3 = (P^2 + F_{ot}P)[(F_{oq}I + (1 - F_{oq}\alpha P_{mo} + F_{oq}Q_{do} + F_{oq}P_f^2)P - (\alpha P_{mo} - Q_{do} - P_f^2)P^2)]^{-1}$, and $Z_3 = N_3 d^T [(F_{oq}I + (1 - F_{oq}\alpha P_{mo} + F_{oq}Q_{do} + F_{oq}P_f^2)P - (\alpha P_{mo} - Q_{do} - P_f^2)P^2)]^{-1}$. Equations (57–59) are Sylvester equations. After solving these Sylvester equations, we get the unknown value of the coefficient vector C_y^T and substituting these values of C_y^T in Eq. (56). We now obtain required non-dimensional temperature $\theta(x, F_o)$ in each layer of skin. Mathematica [41] and MATLAB [42] software has been used for computational analysis.

Results and discussion

To analyze the effect of different parameters and non-Fourier boundary conditions on multi-layer of skin injuries, we select reference value including content properties and parameters as mentioned in Table 1 and some other parameters vary as shown inside the figures.

Comparison with an exact solution

To verify the validity of the method, the solution obtained from FELWGM is compared with the exact solution, which was obtained by using a Laplace transformation technique for a particular case (setting $F_{oq} = F_{ot} = 0$ in Eqs. (18–20) with first kind boundary condition). Using the Laplace transform technique, we obtain the exact solution as follows:

Epidermis layer:

$$\begin{aligned} \theta(x, F_o) = & \frac{1}{U_{1,1}(U_{1,2} + 1)V_1} [-(U_{1,2} + U_{1,3})Q_{do}\theta_w \\ & + P_{mo}(\alpha(U_{1,2} + U_{1,3})\theta_w + (U_{1,1} - 1)(U_{1,1} - U_{1,2})) \\ & + (U_{1,2} - U_{1,1})(U_{1,1} - 1)Q_{vo}] \\ & + \sum_{n=0}^{\infty} \left(\frac{1}{U_{1,4}V_{1,n}} \right) [e^{F_o V_{1,n} - U_{1,4}(x+2)} ((e^{2U_{1,4}x} + e^{2U_{1,4}})\theta_w(Q_{do} + V_{1,n}) \\ & + P_{mo}((e^{2U_{1,4}} - e^{U_{1,4}x})(e^{U_{1,4}x} - 1) - \alpha(e^{2U_{1,4}x} + e^{2U_{1,4}})\theta_w) \\ & + Q_{vo}(-(e^{2U_{1,4}} - e^{U_{1,4}x})(e^{U_{1,4}x} - 1))], \end{aligned} \tag{60}$$

Dermis layer:

$$\begin{aligned} \theta(x, F_o) = & -\frac{1}{U_{2,1}(U_{2,2} + 1)V_2} [(U_{2,2} + U_{2,3})Q_{do}\theta_w \\ & + P_f^2((U_{2,2} - U_{2,1})(-1 + U_{2,1})\theta_b + (U_{2,2} + U_{2,3})\theta_w) \\ & + P_{mo}((U_{2,2} - U_{2,1})(-1 + U_{2,1}) - (U_{2,2} + U_{2,3})\alpha\theta_w)] \\ & + \sum_{n=0}^{\infty} \frac{1}{U_{2,4}V_{2,n}} [e^{F_o V_{2,n} - U_{2,4}(x+2)} ((e^{2U_{2,4}x} + e^{2U_{2,4}}) \\ & \theta_w(Q_{do} + V_{2,n}) + P_f^2((e^{2U_{2,4}} - e^{U_{2,4}x})(e^{U_{2,4}x} - 1)\theta_b \\ & + (e^{2U_{2,4}x} + e^{2U_{2,4}})\theta_w) + P_{mo}((e^{2U_{2,4}} - e^{U_{2,4}x}) \\ & (e^{U_{2,4}x} - 1) - (e^{2U_{2,4}x} + e^{2U_{2,4}})\alpha\theta_w)], \end{aligned} \tag{61}$$

Subcutaneous layer:

$$\begin{aligned} \theta(x, F_o) = & -\frac{1}{U_{3,1}(U_{3,2} + 1)V_3} \\ & [(U_{3,2} + U_{3,3})Q_{do}\theta_w + P_f^2((U_{3,2} - U_{3,1})(-1 + U_{3,1})\theta_b \\ & + (U_{3,2} + U_{3,3})\theta_w) \\ & + P_{mo}((U_{3,2} - U_{3,1})(-1 + U_{3,1}) - (U_{3,2} + U_{3,3})\alpha\theta_w)] \\ & + \sum_{n=0}^{\infty} \frac{1}{U_{3,4}V_{3,n}} [e^{F_o V_{3,n} - U_{3,4}(x+2)} ((e^{2U_{3,4}x} + e^{2U_{3,4}}) \\ & \theta_w(Q_{do} + V_{3,n}) + P_f^2((e^{2U_{3,4}} - e^{U_{3,4}x})(e^{U_{3,4}x} - 1)\theta_b \\ & + (e^{2U_{3,4}x} + e^{2U_{3,4}})\theta_w) \\ & + P_{mo}((e^{2U_{3,4}} - e^{U_{3,4}x})(e^{U_{3,4}x} - 1) \\ & - (e^{2U_{3,4}x} + e^{2U_{3,4}})\alpha\theta_w)], \end{aligned} \tag{62}$$

where $U_{y,4} = \sqrt{-V_y + V_{y,n}}$, $V_1 = \alpha P_{mo} - Q_{do}$, $V_2 = -(P_f^2 - \alpha P_{mo} + Q_{do})$, $V_3 = -(P_f^2 - \alpha P_{mo} + Q_{do})$, $V_{y,n} = \frac{-1}{4}(1 + 2n)^2 \pi^2 + V_y$; $y = 1$ for epidermis, $y = 2$ for dermis, and $y = 3$ for subcutaneous layers. A comparison of the exact and obtained solution is shown in Figs. 2–4 and found in good agreement.

Lagging behavior on skin layer for first kind non-Fourier boundary condition

Epidermis layer: If $F_{oq} = 0, 0.00696379$ and $F_{ot} = 0, 0.00696379$, we observed that the skin temperature decreases continuously. As time decreased, we observed that the temperature of the skin layer in the DPL model is decreased more than both classical Fourier and SPL models as shown in Figs. 5, 8 and 11.

If $\theta_w = 0.229189 = 45.48^\circ C$, the skin layer thickness burns up to $x = 0.3$, here in classical Fourier and SPL models burning are slightly greater than the DPL model. If $\theta_w \geq 0.3 = 48.1^\circ C$, then skin layer burned almost completely. If θ_w increases, we observed that the burning of the skin layer in the DPL model is slightly less than to SPL and classical Fourier model as shown in Fig. 14.

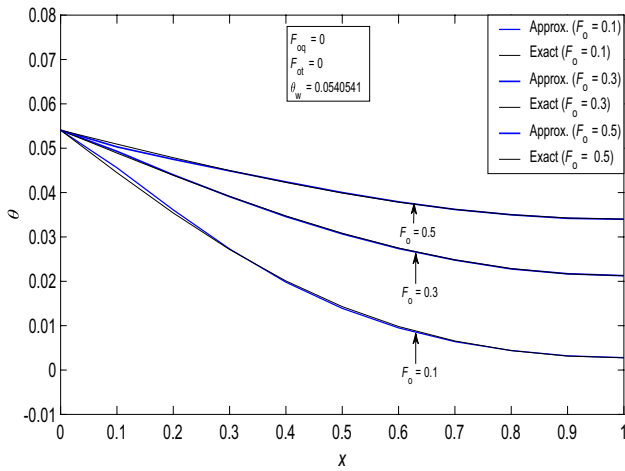


Fig. 2 Epidermis layer: Comparison of exact with approx solution

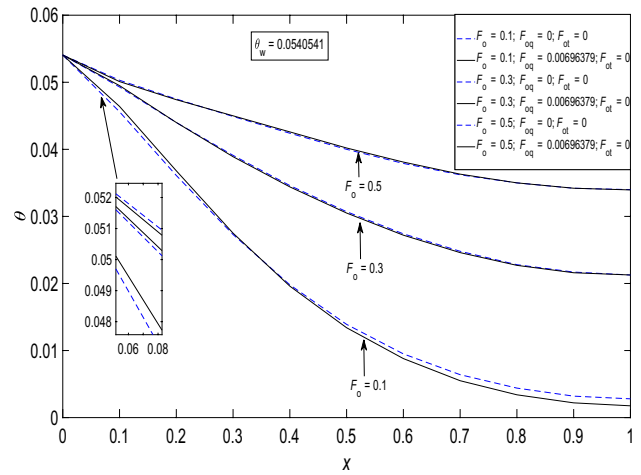


Fig. 5 Epidermis layer: Effect of $F_{oq} = 0.00696379$ and $F_{ot} = 0$ on skin temperature with the first kind non-Fourier boundary condition

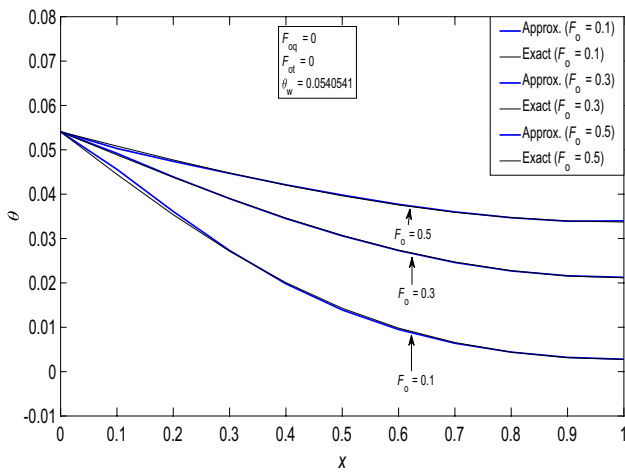


Fig. 3 Dermis layer: Comparison of exact with approx solution

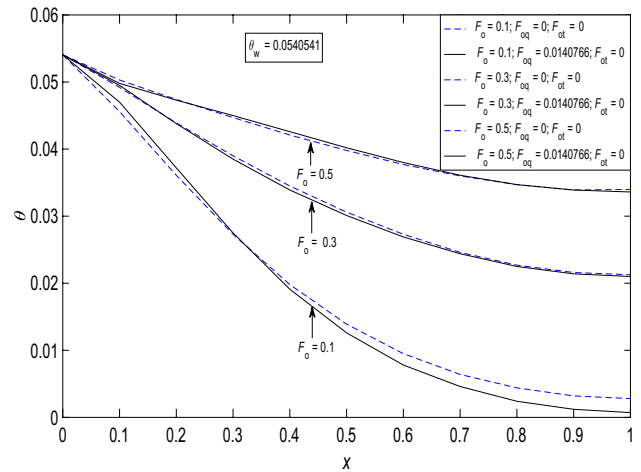


Fig. 6 Dermis layer: Effect of $F_{oq} = 0.0140766$ and $F_{ot} = 0$ on skin temperature with the first kind non-Fourier boundary condition

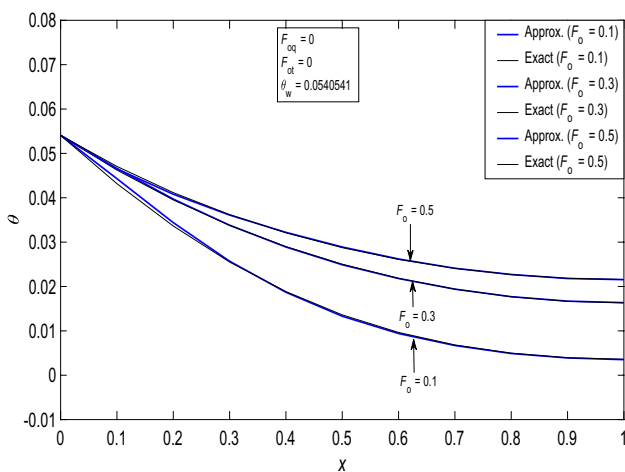


Fig. 4 Subcutaneous layer: Comparison of exact with approx solution

If $F_{oq} = 0.00696379$ be fixed, we observed that damage to skin thickness decreases as F_{ot} increases. If $F_{ot} = 0.00696379$ be fixed, we observed that damage of skin thickness increases as F_{oq} increases as shown in Fig. 32.

Dermis layer: If $F_{oq} = 0, 0.0140766$ and $F_{ot} = 0, 0.0140766$, we observed that the skin temperature decreases continuously. As time decreases, we observed that the temperature of the skin layer in the DPL model is decreased more than both classical Fourier and SPL models. It also observed that initially, ($x = 0.0 - 0.25$) temperature on the skin layer in the DPL model is slowly decreased than both classical Fourier and SPL models, after that skin

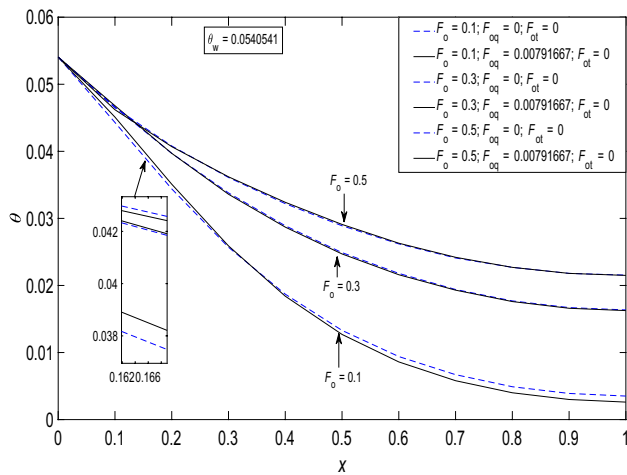


Fig. 7 Subcutaneous layer: Effect of $F_{oq} = 0.00791667$ and $F_{ot} = 0$ on skin temperature with the first kind non-Fourier boundary condition

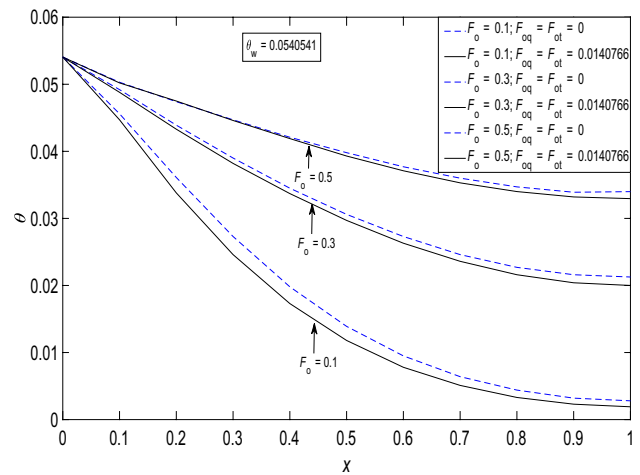


Fig. 9 Dermis layer: Effect of $F_{oq} = F_{ot} = 0.0140766$ on skin temperature with the first kind non-Fourier boundary condition

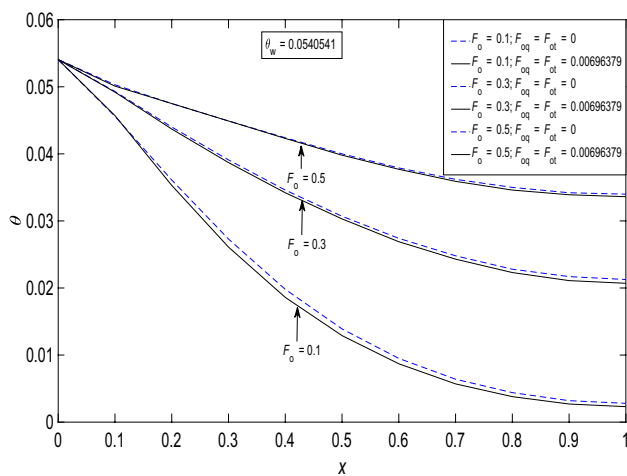


Fig. 8 Epidermis layer: Effect of $F_{oq} = F_{ot} = 0.00696379$ on skin temperature with the first kind non-Fourier boundary condition

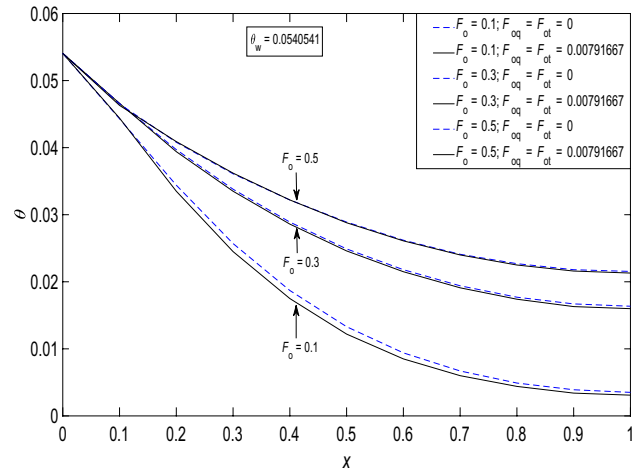


Fig. 10 Subcutaneous layer: Effect of $F_{oq} = F_{ot} = 0.00791667$ on skin temperature with the first kind non-Fourier boundary condition

temperature in the DPL model is below than the both classical Fourier model and SPL model as shown in Figs. 6, 9 and 12.

If $\theta_w = 0.240541 = 45.9^\circ C$, the skin layer thickness burns almost up to $x = 0.4$ in the DPL model with a slight change in classical Fourier and SPL models. If $\theta_w \geq 0.302703 = 48.2^\circ C$, the skin layer burned almost completely. If θ_w increases, we observed that the burning of the skin layer in the DPL model is slightly less than classical Fourier and SPL models as shown in Fig. 15.

If $F_{oq} = 0.0140766$ is fixed, we observed that damage to skin thickness decreases as F_{ot} increases. If $F_{ot} = 0.0140766$

is fixed, in this case, we observed that damage of skin thickness increases as F_{oq} increases as shown in Fig. 33.

Subcutaneous layer: If $F_{oq} = 0, 0.00791667$ and $F_{ot} = 0, 0.00791667$, we observed that the skin temperature decreases continuously. As time decreases, we observed that temperature of the skin layer in the DPL model is decreased more than both classical Fourier and SPL models. It also observed that initially, ($x = 0.0 - 0.3$) skin temperature of the DPL model slight changed with respect to classical Fourier and SPL models, after that skin temperature in DPL model is below than the both classical Fourier and SPL models as shown in Figs. 7, 10 and 13.

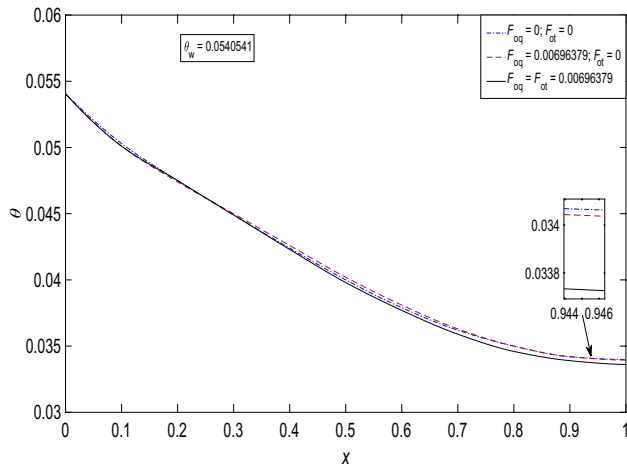


Fig. 11 Epidermis layer: Effect of lagging on skin temperature with the first kind non-Fourier boundary condition at $F_0 = 0.5$

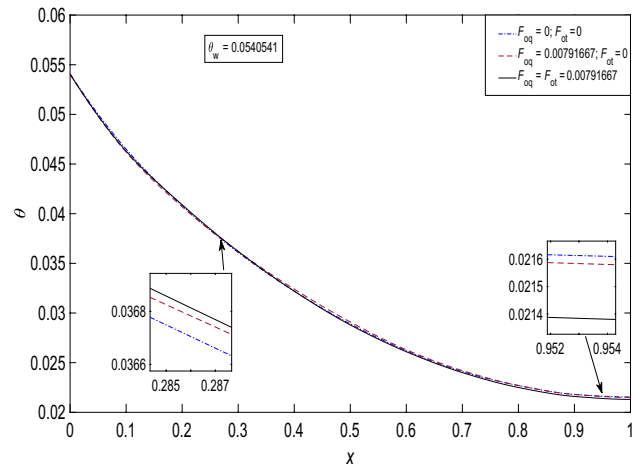


Fig. 13 Subcutaneous layer: Effect of lagging on skin temperature with the first kind non-Fourier boundary condition at $F_0 = 0.5$

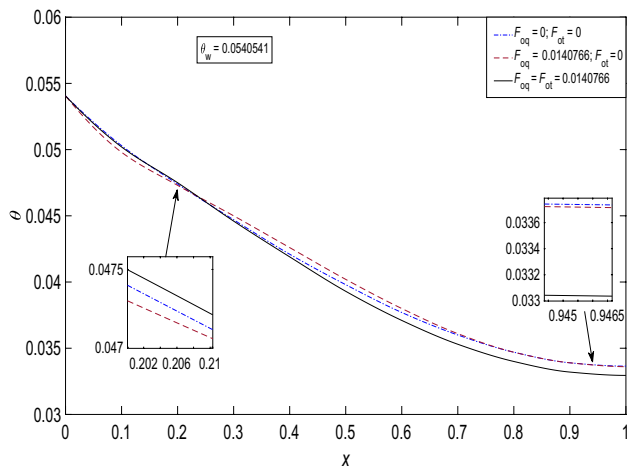


Fig. 12 Dermis layer: Effect of lagging on skin temperature with the first kind non-Fourier boundary condition at $F_0 = 0.5$

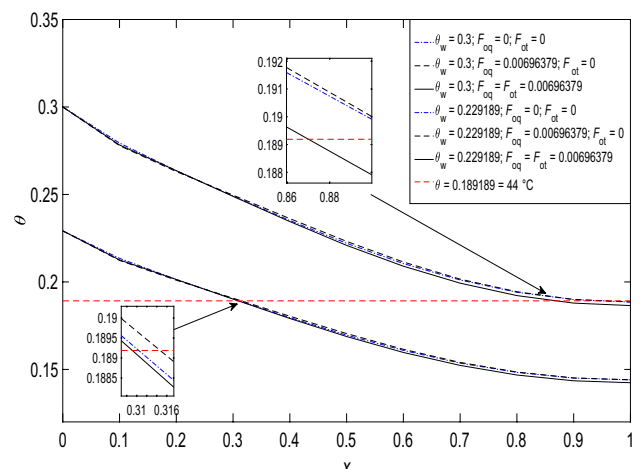


Fig. 14 Epidermis layer: Lagging behavior on skin during different temperature with the first kind non-Fourier boundary condition at $F_0 = 0.5$

If $\theta_w = 0.259459 = 46.6^\circ C$, the skin layer thickness burns almost up to $x = 0.2$ in the DPL model with a slight change in SPL and classical models. If $\theta_w \geq 0.545946 = 57.2^\circ C$, the skin layer burned almost completely. If θ_w increases, we observed that the burning of skin layer in the DPL model is slightly less than classical Fourier and SPL model as shown in Fig. 16.

If $F_{oq} = 0.00791667$ is fixed, we observed that damage to skin thickness increases as F_{ot} increases. If $F_{ot} = 0.00791667$ be fixed, in this case, we observed that damage of skin thickness decreases as F_{oq} increases as shown in Fig. 34.

Effect of temperature on the skin layer thickness for first kind non-Fourier boundary condition

Epidermis, Dermis, and Subcutaneous layers: We found the effect on skin layer thickness for $\theta_w = 0.0540541 (< \theta = 0.189189 (44^\circ C))$, the temperature in the skin layer is constantly increased as time increased and also observed that the temperature rise is less in DPL model than classical Fourier model at the initial time. It has been observed that if the thickness of the skin layer increases, then its temperature decreases as shown in Figs. 17–19 respectively.

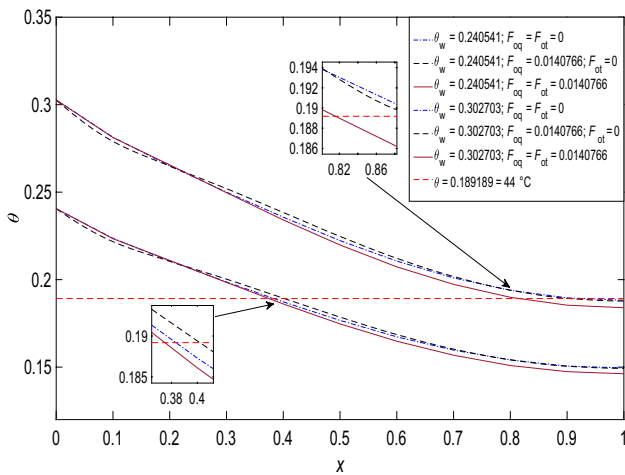


Fig. 15 Dermis layer: Lagging behavior on skin during different temperature with the first kind non-Fourier boundary condition at $F_o = 0.5$

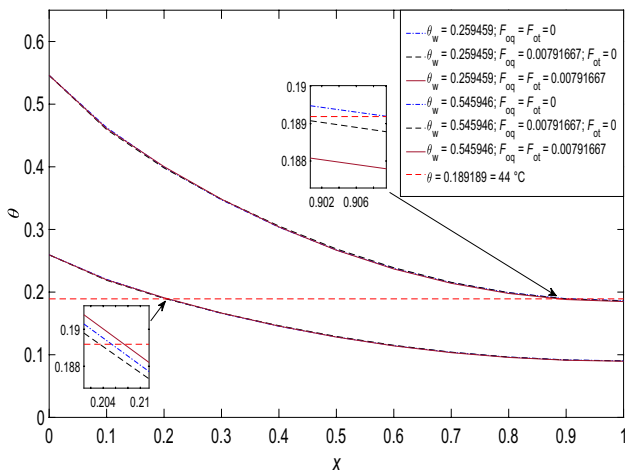


Fig. 16 Subcutaneous layer: Lagging behavior on skin during different temperature with the first kind non-Fourier boundary condition at $F_o = 0.5$

Analysis of lagging on skin during hot and cold surface temperature with the first kind non-Fourier boundary condition at $F_o = 0.5$

Epidermis, Dermis, and Subcutaneous layers: If $\theta_w = 0.0810811 = 40^\circ C (> \text{body temperature})$, we observed that the skin temperature decreases continuously and also found that the skin temperature in the DPL model decreases slightly more than classical Fourier and SPL models. If $\theta_w (= \text{body temperature})$, we found that the temperature has a negligible effect on the skin layer. But if $\theta_w = -0.324324$, we observed that the skin temperature increases continuously because the layer temperature reaches to normal body

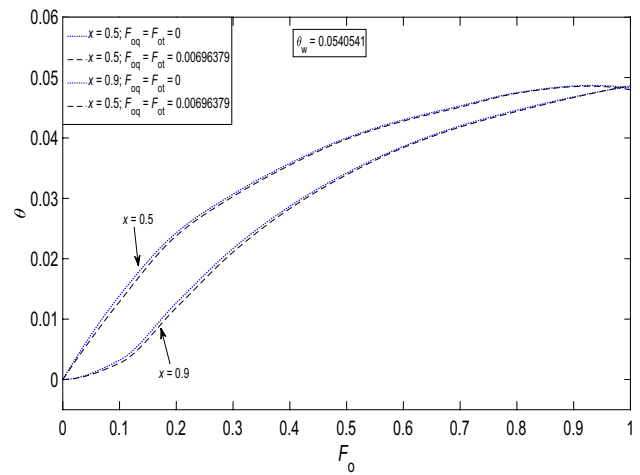


Fig. 17 Epidermis layer: The effect on skin thickness between temperature and time with the first kind non-Fourier boundary condition

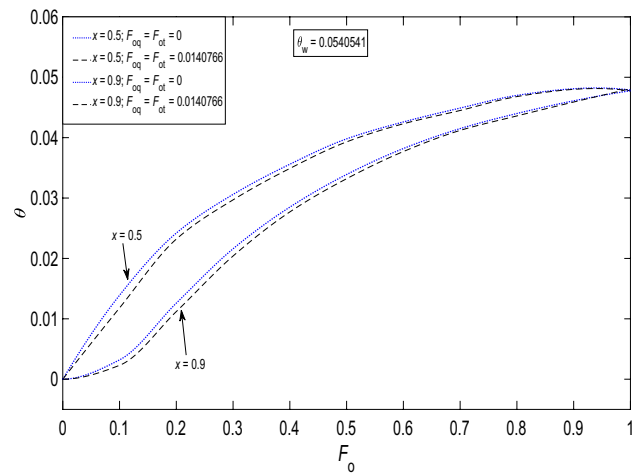


Fig. 18 Dermis layer: The effect on skin thickness between temperature and time with the first kind non-Fourier boundary condition

temperature and also found that the skin temperature in the DPL model increases slightly more than classical Fourier and SPL models as shown in Figs. 20–22, respectively.

Effect of Kirchoff number (K_i) and Biot number (B_i) on skin layer at $F_o = 0.5$

The non-dimensional quantity K_i is defined by the reference heat flux on the temperature profile that is demonstrated in the second kind boundary condition. We observed that as the value of the K_i increased at fixed $F_o = 0.5$, then the temperature of the skin increases at the initial boundary position, i.e., $x = 0$. At a fixed Kirchoff number, we observed that the skin temperature is decreasing continuously as $x > 0$ which is shown in Figs. 23–25.

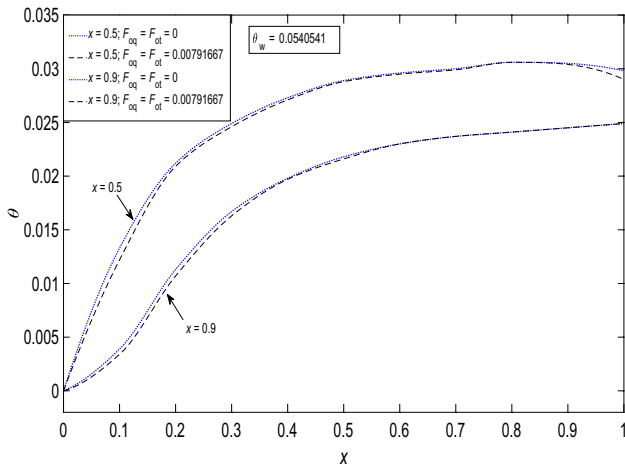


Fig. 19 Subcutaneous layer: The effect on skin thickness between temperature and time with the first kind non-Fourier boundary condition

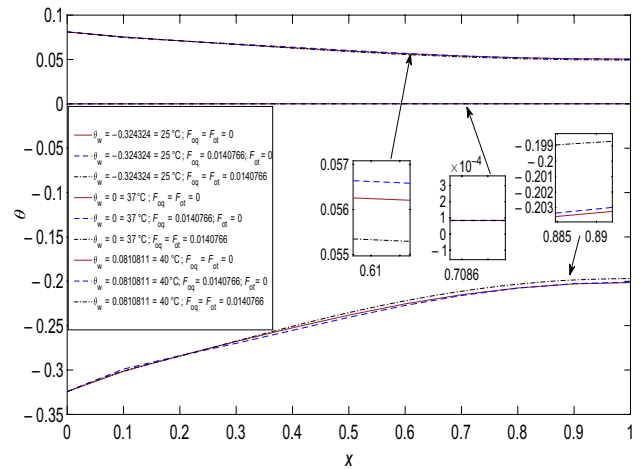


Fig. 21 Dermis layer: Effect of lagging on skin during hot and cold temperature

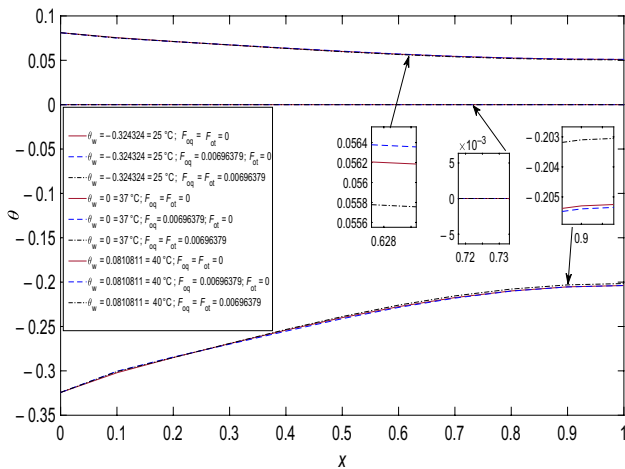


Fig. 20 Epidermis layer: Effect of lagging on skin during hot and cold temperature

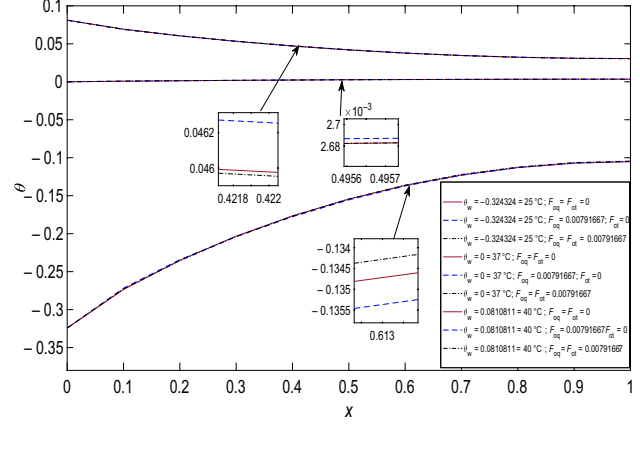


Fig. 22 Subcutaneous layer: Effect of lagging on skin during hot and cold temperature

The non-dimensional quantity B_i is defined by the reference heat transfer coefficient which is demonstrated in the third kind boundary condition. We observed that as the value of the B_i increased at fixed $F_o = 0.5$, then the temperature of the skin increases at the initial boundary position, i.e., $x = 0$. At a fixed Biot number, we observed that the skin temperature is decreasing continuously as $x > 0$ which is shown in Figs. 26–28.

The effect of generalized non-Fourier boundary condition on three layers of skin at $F_o = 0.5$

Epidermis, Dermis, and Subcutaneous layer: In the first, second, and third kind non-Fourier boundary conditions, we

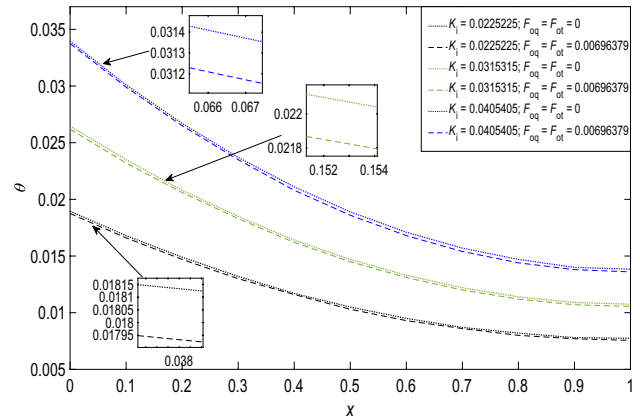


Fig. 23 Epidermis layer: K_i effect on skin

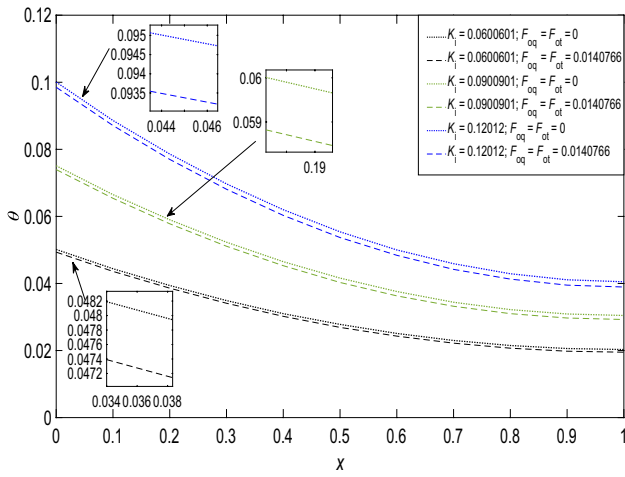


Fig. 24 Dermis layer: K_i effect on skin

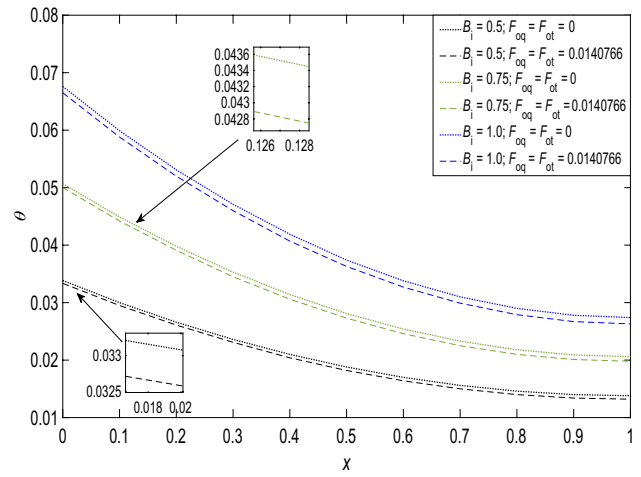


Fig. 27 Dermis layer: B_i effect on skin

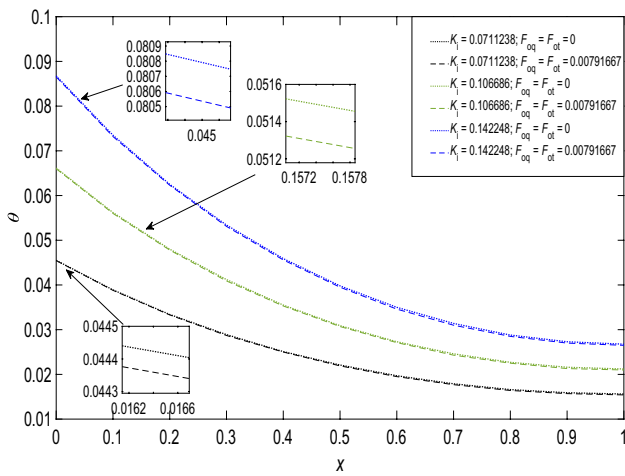


Fig. 25 Subcutaneous layer: K_i effect on skin

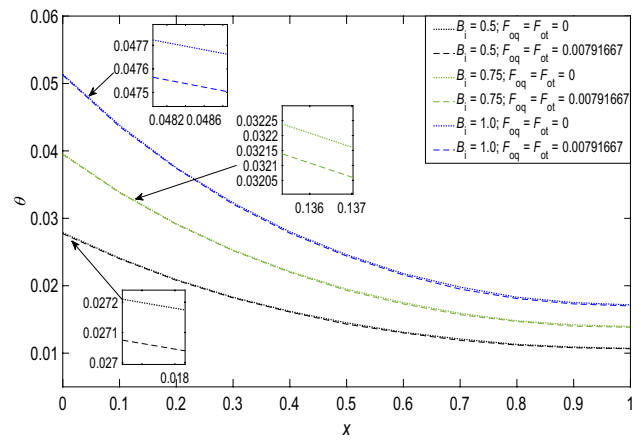


Fig. 28 Subcutaneous layer: B_i effect on skin

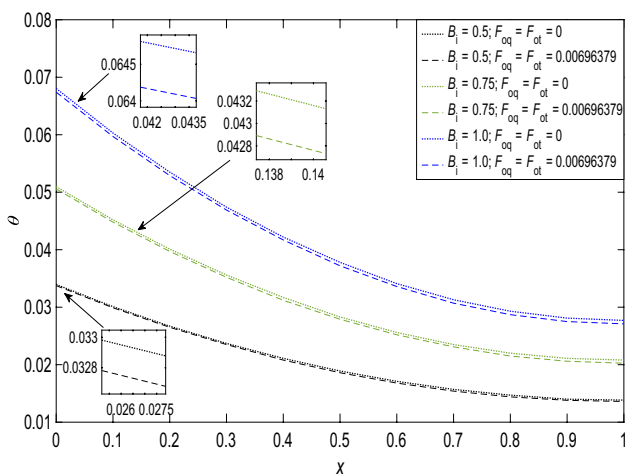


Fig. 26 Epidermis layer: B_i effect on skin

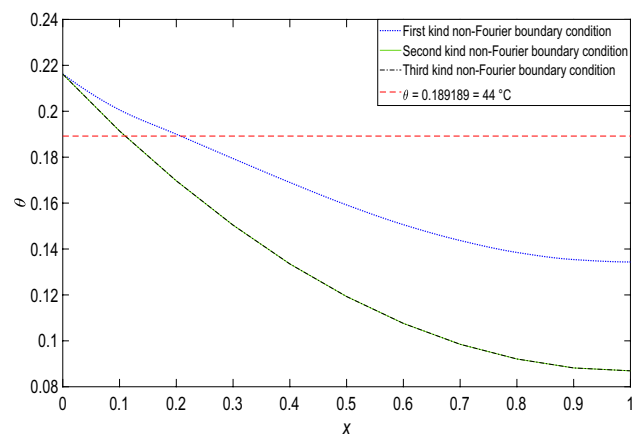


Fig. 29 Epidermis layer: Effect of temperature on skin during non-Fourier generalized boundary condition

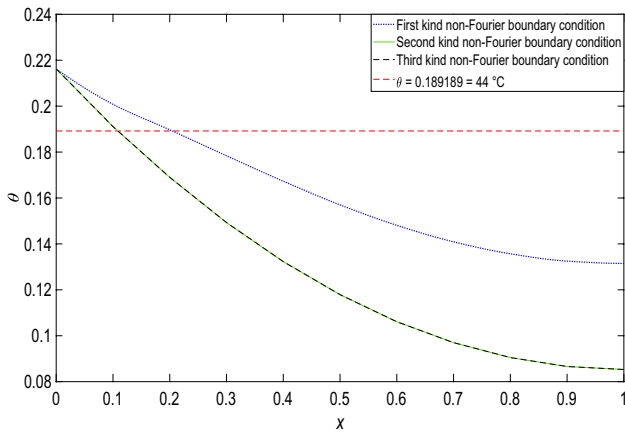


Fig. 30 Dermis layer: Effect of temperature on skin during non-Fourier generalized boundary condition

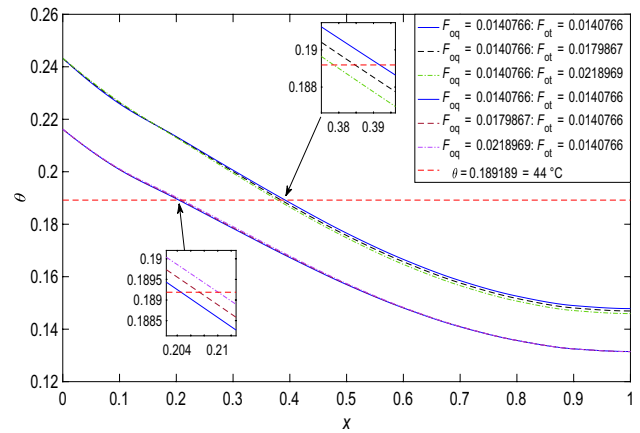


Fig. 33 Dermis layer: Effect of lagging on skin temperature with the first kind non-Fourier boundary condition

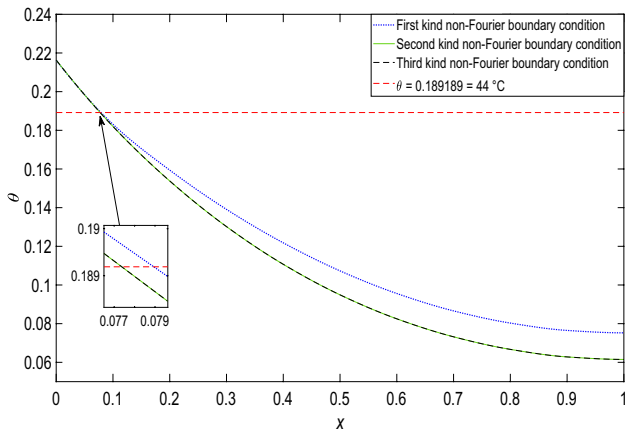


Fig. 31 Subcutaneous layer: Effect of temperature on skin during non-Fourier generalized boundary condition

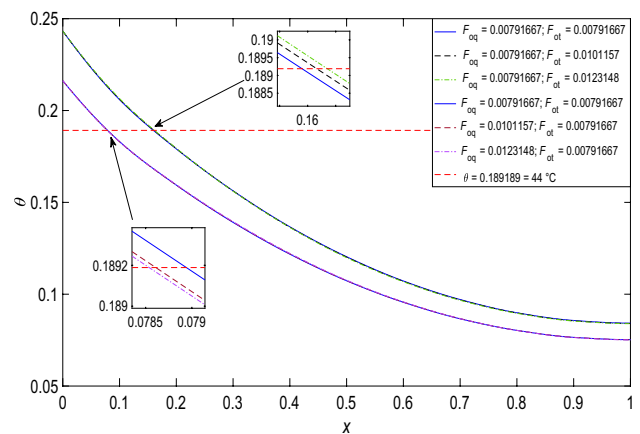


Fig. 34 Subcutaneous layer: Effect of lagging on skin temperature with the first kind non-Fourier boundary condition

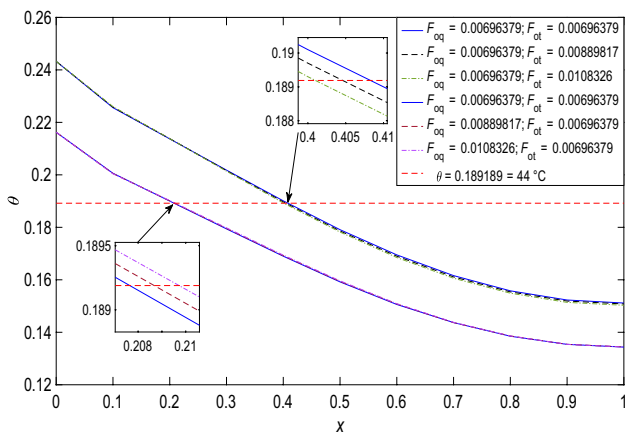


Fig. 32 Epidermis layer: Effect of lagging on skin temperature with the first kind non-Fourier boundary condition

observed that skin temperature is continuously decreased. The skin layer temperature in the second and third kind non-Fourier boundary conditions decreases fast in comparison with the first kind non-Fourier boundary condition as shown in Figs. 29–31, respectively.

Conclusions

In this work, a detailed description of skin burns on different types of non-Fourier boundary condition is considered. The Legendre wavelet properties are applied to calculate the approximate analytical solution of the DPL model of multi-layer of skin.

In the first kind non-Fourier boundary condition, the burning of the skin layers depends on its thickness. As skin layer thickness increases, then burning reduces.

The burning time for skin layers varies with temperatures. As time increases, burning of the skin layers thickness also increases.

The temperature on skin layers decreases continuously in non-Fourier generalized boundary condition. In epidermis and dermis layers, the first kind non-Fourier boundary condition has more difference in the burning of skin layer thickness in comparison with the second and third kind non-Fourier boundary conditions. In subcutaneous layer, the first kind non-Fourier boundary condition has little difference in the burning of skin layer thickness in comparison with the second and third kind non-Fourier boundary conditions.

The skin layer thickness in the DPL model is less damaged than both classical Fourier and SPL models. If $\theta_w >$ body temperature, we observed that skin temperature in the DPL model is significantly decreased in comparison with classical Fourier and SPL models. If $\theta_w <$ body temperature, we observed that skin temperature in the DPL model is significantly increased in comparison with classical Fourier and SPL models because the layer temperature reaches to normal body temperature.

At time $F_o = 0.5$, the multi-layer of skin thickness is completely burned if surface temperature θ_w is greater than θ_b

$$\text{where } \theta_b = \begin{cases} 0.3 = 48.1^\circ\text{C} & \text{For Epidermis layer. i.e. First Kind Burn,} \\ 0.302703 = 48.2^\circ\text{C} & \text{For Dermis layer. i.e. Second Kind Burn,} \\ 0.545946 = 57.2^\circ\text{C} & \text{For Subcutaneous layer. i.e. Third Kind Burn.} \end{cases}$$

The burning of skin thickness decreases if

$$\begin{cases} F_{oq} < F_{ot} & \text{For Epidermis layer,} \\ F_{oq} < F_{ot} & \text{For Dermis layer, and} \\ F_{oq} > F_{ot} & \text{For Subcutaneous layer.} \end{cases}$$

The burning of skin thickness increases if

$$\begin{cases} F_{oq} > F_{ot} & \text{For Epidermis layer,} \\ F_{oq} > F_{ot} & \text{For Dermis layer, and} \\ F_{oq} < F_{ot} & \text{For Subcutaneous layer.} \end{cases}$$

The present work demonstrates the study of the DPL model of multi-layer of skin based on heat transfer and FELWGM as a solution method helps in the precise prediction of temperature. So, it makes this study more useful for the prediction and control of temperature for medical doctors in the clinical field. The entire analysis is presented in non-dimensional form. Therefore, these results provide a more comprehensive and better insight for understanding the behavior of skin burn injuries during temperature distribution of different types of boundary condition.

Acknowledgements First author would like to thanks the CSIR, New Delhi, India, for the financial support under the JRF (09/013(0931)/2020-EMR-I) scheme and also to the Department of Mathematics (Institute of Science), Banaras Hindu University (BHU), Varanasi (U.P), India, for providing necessary facilities. We thank all anonymous reviewers for spending valuable time to give valuable comments so that our manuscript is improved in the present form.

Appendix

Second kind non-Fourier boundary condition

From Eq. (23), we have found the second kind non-Fourier boundary condition, i.e.,

$$\frac{\partial}{\partial x} \left[\theta(x, F_o) + F_{ot} \frac{\partial \theta(x, F_o)}{\partial F_o} \right] = -K_i \quad \text{at } x = 0. \tag{63}$$

Taking the Laplace transform of Eq. (63), we obtained

$$\frac{\partial}{\partial x} \left[\tilde{\theta}(x, s) + F_{ot} \{s\tilde{\theta}(x, s) - \theta(x, 0)\} \right] = -\frac{K_i}{s} \quad \text{at } x = 0. \tag{64}$$

Using initial condition $\theta(x, 0) = 0$ in Eq. (64), we get

$$\frac{\partial}{\partial x} \left[\tilde{\theta}(x, s) + F_{ot}s\tilde{\theta}(x, s) \right] = -\frac{K_i}{s} \quad \text{at } x = 0, \tag{65}$$

$$(1 + F_{ot}s) \frac{\partial \tilde{\theta}(x, s)}{\partial x} = -\frac{K_i}{s} \quad \text{at } x = 0, \tag{66}$$

$$\frac{\partial \tilde{\theta}(x, s)}{\partial x} = -\frac{K_i}{s(1 + F_{ot}s)} \quad \text{at } x = 0. \tag{67}$$

Inverse Laplace transform of Eq. (67) is

$$\frac{\partial \theta(x, F_o)}{\partial x} = -K_i(1 - e^{-\frac{F_o}{F_{ot}}}) \quad \text{at } x = 0. \tag{68}$$

Third kind non-Fourier boundary condition

From Eq. (23), we have found third kind non-Fourier boundary condition, i.e.,

$$\frac{\partial}{\partial x} \left[\theta(x, F_o) + F_{ot} \frac{\partial \theta(x, F_o)}{\partial F_o} \right] - B_i \theta(x, F_o) = -B_i \theta_s \quad \text{at } x = 0, \tag{69}$$

$$\frac{\partial}{\partial x} \left[\theta(x, F_o) + F_{ot} \frac{\partial \theta(x, F_o)}{\partial F_o} \right] = -B_i(\theta_s - \theta(x, F_o)) \quad \text{at } x = 0. \tag{70}$$

Taking the Laplace transform of Eq. (70), we obtained

$$\frac{\partial}{\partial x} [\tilde{\theta}(x, s) + F_{ot}\{s\tilde{\theta}(x, s) - \theta(x, 0)\}] = -B_i(\theta_s - \theta(x, s)) \quad \text{at } x = 0. \tag{71}$$

Using initial condition $\theta(x, 0) = 0$ in Eq. (71), we get

$$\frac{\partial}{\partial x} \left[\tilde{\theta}(x, s) + F_{ot}s\tilde{\theta}(x, s) \right] = \frac{-B_i(\theta_s - \theta(x, s))}{s} \quad \text{at } x = 0, \tag{72}$$

$$(1 + F_{ot}s) \frac{\partial \tilde{\theta}(x, s)}{\partial x} = \frac{-B_i(\theta_s - \theta(x, s))}{s} \quad \text{at } x = 0, \quad (73)$$

$$\frac{\partial \tilde{\theta}(x, s)}{\partial x} = \frac{-B_i(\theta_s - \theta(x, s))}{s(1 + F_{ot}s)} \quad \text{at } x = 0. \quad (74)$$

Inverse Laplace transform of Eq. (74) is

$$\frac{\partial \theta(x, F_o)}{\partial x} = -B_i(\theta_s - \theta(x, F_o))(1 - e^{-\frac{F_o}{F_{ot}}}) \quad \text{at } x = 0. \quad (75)$$

Non-Fourier symmetric condition

From Eq. (27), we have found non-Fourier symmetric condition, i.e.,

$$\frac{\partial}{\partial x} \left[\theta(x, F_o) + F_{ot} \frac{\partial \theta(x, F_o)}{\partial F_o} \right] = 0 \quad \text{at } x = 1. \quad (76)$$

Taking the Laplace transform of Eq. (76), we obtained

$$\frac{\partial}{\partial x} [\tilde{\theta}(x, s) + F_{ot} \{s\tilde{\theta}(x, s) - \theta(x, 0)\}] = 0 \quad \text{at } x = 1. \quad (77)$$

Using initial condition $\theta(x, 0) = 0$ in Eq. (77), we get

$$\frac{\partial}{\partial x} [\tilde{\theta}(x, s) + F_{ot}s\tilde{\theta}(x, s)] = 0 \quad \text{at } x = 1, \quad (78)$$

$$(1 + F_{ot}s) \frac{\partial \tilde{\theta}(x, s)}{\partial x} = 0 \quad \text{at } x = 1, \quad (79)$$

$$\frac{\partial \tilde{\theta}(x, s)}{\partial x} = 0 \quad \text{at } x = 1. \quad (80)$$

Inverse Laplace transform of Eq. (80) is

$$\frac{\partial \theta(x, F_o)}{\partial x} = 0 \quad \text{at } x = 1. \quad (81)$$

References

- Pennes HH. Analysis of tissue and arterial blood temperature in the resting human forearm. *J Appl Physiol.* 1948;1:93–122.
- Weinbaum S, Jiji LM. A new simplified bioheat equation for the effect of blood flow on local average tissue temperature. *ASME J Biomech Eng.* 1985;107:131–9.
- Nakayama A, Kuwahara F. A general bioheat transfer model based on the theory of porous media. *Int J Heat Mass Transf.* 2008;51:3190–9.
- Shen WS, Zhang J, Yang FQ. Skin thermal injury prediction with strain energy. *Int J Nonlinear Sci Numer Simul.* 2005;6:317–28.
- Duncan JM, David CE, Richard A. Dynamic simulations of tissue welding. *Proc SPIE.* 1996;2671:234–42.
- Ming F, Weng W, Yuan H. Numerical simulation of the effects of blood perfusion, water diffusion, and vaporization on the skin temperature and burn injuries. *Numer Heat Transf Part A.* 2014;65:1187–203.
- Ming F, Chen W, Weng W, Yuan M, Luo N, Xu X. Prediction of thermal skin burn based on the combined mathematical model of the skin and clothing. *J Textile Inst.* 2018;109(12):1606–12.
- Peng J, Tian Y. A surface heat disturbance method for measuring local tissue blood perfusion rate. *J Therm Sci.* 1996;5(1):28–33.
- Chen B, Zhang Y, Li D. Numerical investigation of the thermal response to skin tissue during laser lipolysis. *J Therm Sci.* 2018;27(5):470–8.
- Gupta PK, Singh J, Rai KN. Numerical simulation for heat transfer in tissues during thermal therapy. *J Therm Biol.* 2010;35(6):295–301.
- Gupta PK, Singh J, Rai KN. A numerical study on heat transfer in tissues during hyperthermia. *Math Comput Model.* 2013;57:1018–37.
- Cattaneo C. A form of heat conduction equation which eliminates the paradox of instantaneous propagation. *C R Acad Sci.* 1958;247:431–3.
- Vernotte P. Les paradoxes de la theorie continue de l'equation de la chaleur. *C R Acad Sci.* 1958;246:3154–5.
- Liu KC. Thermal propagation analysis for living tissue with surface heating. *Int J Therm Sci.* 2008;47:507–13.
- Kumar D, Kumar P, Rai KN. Numerical study on non-Fourier bio heat transfer during thermal ablation, vol. 127. Amsterdam: Elsevier; 2015. p. 1300–7.
- Upadhyay S, Rai KN. Finite element Legendre wavelet Galerkin approach in investigation of non-Fourier's and non-Ficks's effects on heat and mass transfer during drying of foods. *Comput Therm Sci Int J.* 2018;10:493–519.
- Bhattacharyya A, Seth GS, Kumar R, Chamkha AJ. Simulation Cattaneo–Christov heat flux on the flow of single and multi-walled carbon nanotubes between two stretchable coaxial rotating disks. *J Therm Anal Calorim.* 2020;139:1655–70.
- Tzou DY. A unified field approach for heat conduction from macro-to microscales. *J Heat Transf.* 1995;117(1):8–16.
- Tzou DY. Macro- to-microscale heat transfer: the lagging behavior. Washington DC: Taylor and Francis; 1996.
- Zhang Y. Generalized dual-phase lag bioheat equations based on nonequilibrium heat transfer in living biological tissues. *Int J Heat Mass Transf.* 2009;52:4829–34.
- Kumar P, Kumar D, Rai KN. A numerical study on dual-phase-lag model of bioheat transfer during hyperthermia treatment. *J Therm Biol.* 2015;49:98–105.
- Kumar P, Kumar D, Rai KN. Numerical simulation of dual-phase-lag bioheat transfer model during thermal therapy. *Math Biosci.* 2016;281:82–91.
- Odibat Z, Kumar S. A robust computational algorithm of homotopy asymptotic method for solving systems of fractional differential equations. *J Comput Nonlinear Dynam.* 2019;14(8):081004.
- Ajou AEI, Oqielat MN, Zhou ZA, Kumar S, Momani S. Solitary solutions for time-fractional nonlinear dispersive PDEs in the sense of conformable fractional derivative. *Chaos.* 2019;29:093102.
- Emile F, Doungmo G, Kumar S, Mugisha SB. Similarities in a fifth-order evolution equation with and with no singular kernel. *Chaos Solitons Fractals.* 2020;130:109467.
- Kumar S, Kumar A, Momani S, Aldhaifallah M, Nisar KS. Numerical solutions of nonlinear fractional model arising in the appearance of the strip patterns in two-dimensional systems. *Adv Differ Equ.* 2019;2019:413.

27. Sharma B, Kumar S, Cattani C, Baleanu D. Nonlinear dynamics of Cattaneo–Christov heat flux model for third-grade power-law fluid. *J Comput Nonlinear Dyn*. 2019;1131.
28. Yanying X, Chao L, Ruiqing S, Zhi W, Qingsheng W. Experimental investigation of thermal properties and fire behavior of carbon/epoxy laminate and its foam core sandwich composite. *J Therm Anal Calorim*. 2019;136:1237–47.
29. Kleilton OS, Rossemerg CB, Josué SB, André GBJ, Wladymyr JBS, Sandra MCB, Rodrigo JO, Marcus VLF. Thermal, chemical, biological and mechanical properties of chitosan films with powder of eggshell membrane for biomedical applications. *J Therm Anal Calorim*. 2019;136:725–35.
30. Henze M, Bogdanic L, Muehlbauer K, Schnieder M. Effect of the Biot number on metal temperature of thermal-barrier-coated turbine parts-real engine measurements. *J Turbomach*. 2013;135:031029.
31. Khalid MZ, Zubair M, Ali M. An analytical method for the solution of two phase Stefan problem in cylindrical geometry. *Appl Math Comput*. 2019;342:295–308.
32. Szafer A, Zhong JH, Gore JC. Theoretical-model for water diffusion in tissues. *Magn Reson Med*. 1995;33:697–712.
33. Jiang SC, Ma N, Li HJ, Zhang XX. Effects of thermal properties and geometrical dimensions on skin burn injuries. *Burns*. 2002;28:713–7.
34. Ng EYK, Chua LT. Prediction of skin burn injury, part 2: parametric and sensitivity analysis. *P I Mech Eng H*. 2002;216:171–83.
35. Johnson NN, Abraham JP, Helgeson ZI, Minkowycz WJ, Sparrow EM. An archive of skin-layer thicknesses and properties and calculations of scald burns with comparisons to experimental observations. *J Therm Sci Eng Appl*. 2011;3:1–9.
36. Henriques FC, Moritz AR. Studies of thermal injuries I: the conduction of heat to and through skin and the temperatures attained therein, a theoretical and experimental investigation. *Am J Pathol*. 1947;23:531–49.
37. Stoll AM, Chianta MA. Method and rating system for evaluation of thermal protection. *Aerospace Med*. 1969;40:1232–7.
38. Weaver JA, Stoll AM. Mathematical model of skin exposed to thermal radiation. *Aerosp Med*. 1969;40:24–30.
39. Scheid F. *Schaum’s outline of theory and problems: numerical analysis*. 2nd ed. New York: McGraw-Hill; 1989.
40. Razzaghi M, Yousefi S. The Legendre wavelets operational matrix of integration. *Int J Syst Sci*. 2001;32(4):495–502.
41. Don E. *Mathematica Second edition, Schaum’s outline’s Series*, ISBN: 978-0-07-160829-9.
42. Prata R. *Getting started with matlab a quick introduction for scientists and engineers*. New York: Oxford University Press; 2010.

Publisher’s Note Springer Nature remains neutral with regard to jurisdictional claims in published maps and institutional affiliations.